Neuropharmacology 95 (2015) 479–491

Contents lists available at ScienceDirect

Neuropharmacology

journal homepage: www.elsevier.com/locate/neuropharm

MAM-2201, a synthetic cannabinoid drug of abuse, suppresses the synaptic input to cerebellar Purkinje cells via activation of presynaptic CB1 receptors

Tomohiko Irie [a, *], Ruri Kikura-Hanajiri [b], Makoto Usami [a], Nahoko Uchiyama [b], Yukihiro Goda [c], Yuko Sekino [a, **]

[a] Division of Pharmacology, National Institute of Health Sciences, Tokyo, Japan
[b] Division of Pharmacognosy, Phytochemistry, and Narcotics, National Institute of Health Sciences, Tokyo, Japan
[c] Division of Drugs, National Institute of Health Sciences, Tokyo, Japan

ARTICLE INFO

Article history:
Received 26 June 2014
Received in revised form
18 December 2014
Accepted 20 February 2015
Available online 5 March 2015

Keywords:
Synthetic cannabinoids
MAM-2201
Cannabinoid receptor type 1
Purkinje cell
Cerebellum
Neurotransmitter release

ABSTRACT

Herbal products containing synthetic cannabinoids—initially sold as legal alternatives to marijuana—have become major drugs of abuse. Among the synthetic cannabinoids, [1-(5-fluoropentyl)-1*H*-indol-3-yl](4-methyl-1-naphthalenyl)-methanone (MAM-2201) has been recently detected in herbal products and has psychoactive and intoxicating effects in humans, suggesting that MAM-2201 alters brain function. Nevertheless, the pharmacological actions of MAM-2201 on cannabinoid receptor type 1 (CB1R) and neuronal functions have not been elucidated. We found that MAM-2201 acted as an agonist of human CB1Rs expressed in AtT-20 cells. In whole-cell patch-clamp recordings made from Purkinje cells (PCs) in slice preparations of the mouse cerebellum, we also found that MAM-2201 inhibited glutamate release at parallel fiber-PC synapses via activation of presynaptic CB1Rs. MAM-2201 inhibited neurotransmitter release with an inhibitory concentration 50% of 0.36 μM. MAM-2201 caused greater inhibition of neurotransmitter release than Δ^9-tetrahydrocannabinol within the range of 0.1–30 μM and JWH-018, one of the most popular and potent synthetic cannabinoids detected in the herbal products, within the range of 0.03–3 μM. MAM-2201 caused a concentration-dependent suppression of GABA release onto PCs. Furthermore, MAM-2201 induced suppression of glutamate release at climbing fiber-PC synapses, leading to reduced dendritic Ca^{2+} transients in PCs. These results suggest that MAM-2201 is likely to suppress neurotransmitter release at CB1R-expressing synapses in humans. The reduction of neurotransmitter release from CB1R-containing synapses could contribute to some of the symptoms of synthetic cannabinoid intoxication including impairments in cerebellum-dependent motor coordination and motor learning.

Abbreviations: ACSF, artificial cerebrospinal fluid; AM251, *N*-(piperidin-1-yl)-5-(4-iodophenyl)-1-(2,4-dichlorophenyl)-4-methyl-1*H*-pyrazole-3-carboxamide; CB1R, cannabinoid receptor type 1; CB2R, cannabinoid receptor type 2; CF, climbing fiber; CI, confidence interval; CV, coefficient of variation; DNQX, 6,7-dinitroquinoxaline-2,3-dione; EC50, effective concentration 50%; eCBs, endocannabinoids; EGTA, ethylene glycol tetraacetic acid; EPSC, excitatory postsynaptic current; GFP, green fluorescent protein; hCB1R, human CB1R; HEPES, 4-(2-hydroxyethyl)-1-piperazineethanesulfonic acid; IC50, inhibitory concentration 50%; IEI, inter-event interval; IPSC, inhibitory postsynaptic current; JWH-018, naphthalen-1-yl-(1-pentylindol-3-yl)methanone; LTD, long-term depression; MAM-2201, [1-(5-fluoropentyl)-1*H*-indol-3-yl](4-methyl-1-naphthalenyl)-methanone; mCB1R, mouse CB1R; mIPSC, miniature IPSC; OGB-1, Oregon Green 488 BAPTA-1 hexapotassium salt; P, postnatal day; PC, Purkinje cell; PF, parallel fiber; PPR, paired-pulse ratio; qEPSC, quantal EPSC; THC, tetrahydrocannabinol; TTX, tetrodotoxin; WIN, WIN 55,212-2 mesylate, (*R*)-(+)-[2,3-Dihydro-5-methyl-3-(4-morpholinylmethyl)pyrrolo[1,2,3-de]-1,4-benzoxazin-6-yl]-1-naphthalenylmethanone mesylate.

* Corresponding author. Division of Pharmacology, National Institute of Health Sciences, 1-18-1 Kamiyoga, Setagaya-ku, Tokyo 158-8501, Japan. Tel.: +81 3 3700 9762.
** Corresponding author. Division of Pharmacology, National Institute of Health Sciences, 1-18-1 Kamiyoga, Setagaya-ku, Tokyo 158-8501, Japan. Tel.: +81 3 3700 9692.
E-mail addresses: irie@nihs.go.jp (T. Irie), yukos@nihs.go.jp (Y. Sekino).

http://dx.doi.org/10.1016/j.neuropharm.2015.02.025
0028-3908/

1. Introduction

Marijuana (*Cannabis sativa*) has been widely abused for recreational purposes and contains the psychoactive compound Δ^9-tetrahydrocannabinol (Δ^9-THC) (Taura et al., 2007). Δ^9-THC binds to cannabinoid receptors type 1 and 2 (CB1R and CB2R), which are G protein-coupled receptors. CB1Rs are abundantly expressed in the mammalian brain, whereas CB2Rs are expressed mainly in the immune system (Showalter et al., 1996; Mackie, 2008; Kano et al., 2009). The psychoactive effects of Δ^9-THC are mediated by CB1Rs (Huestis et al., 2001; Monory et al., 2007). Starting in the late 2000s, herbal products containing synthetic cannabinoids, which are chemical compounds produced for the purpose of mimicking the effects of Δ^9-THC, became a major class of drugs of abuse, and are sold as alternatives to marijuana around the world (Auwarter et al., 2009; Vardakou et al., 2010; Seely et al., 2012; Kikura-Hanajiri et al., 2013). Among the synthetic cannabinoids, [1-(5-fluoropentyl)-1*H*-indol-3-yl](4-methyl-1-naphthalenyl)-methanone (MAM-2201, Fig. 1*A*) was recently identified in these herbal products (Moosmann et al., 2012; Derungs et al., 2013; Kikura-Hanajiri et al., 2013; Saito et al., 2013; Uchiyama et al., 2013; Lonati et al., 2014). In humans, abuse of products containing MAM-2201 causes a psychotic state with agitation, aggression, and anxiety, and can cause serious harm to the user including death. These reports imply that MAM-2201 exerts potent pharmacological actions on brain functions and causes psychoactive and intoxicating effects. Nevertheless, it remains unknown whether MAM-2201 activates CB1Rs and how MAM-2201 affects neuronal functions such as synaptic transmission.

Endocannabinoids (eCBs) mediate various types of synaptic plasticity throughout the mammalian brain. eCBs are released from postsynaptic neurons in response to synaptic activity and act in a retrograde manner on presynaptic terminals, to suppress neurotransmitter release (Wilson and Nicoll, 2002; Kano et al., 2009; Regehr et al., 2009). The synaptic effects of eCBs are mediated by presynaptic CB1Rs. In presynaptic terminals, activation of CB1Rs mainly inhibits voltage-gated Ca^{2+} channels coupled to exocytosis, leading to a reduction of neurotransmitter release (Brown et al., 2004; Kushmerick et al., 2004).

Numerous neurophysiological and neuropharmacological studies of CB1Rs have been performed on the cerebellum of rodents, which have well-characterized neuronal circuits and play crucial roles in motor coordination and motor learning (Llinas et al., 2004; Kano et al., 2009). In the cerebellum, Purkinje cells (PCs) are the principal GABAergic neurons and provide the sole output from the cerebellar cortex. PCs receive two types of glutamatergic excitatory inputs, climbing fibers (CFs) and parallel fibers (PFs). CFs arise from the inferior olivary complex. Activation of CF-PC synapses induces strong postsynaptic depolarization, which evokes a dendritic Ca^{2+} transient and complex spikes consisting of a burst of several action potentials (spikelets). PFs are the axons of the granule cells located in the deep layers of the cerebellum and form numerous *en passant* synapses on the spines of distal dendrites of PCs (Llinas et al., 2004). PCs also receive feed-forward inhibition from GABAergic interneurons in the molecular layer of the cerebellar cortex (Mittmann et al., 2005). Neurotransmitter release at CF-PC, PF-PC, and interneuron-PC synapses is suppressed via activation of presynaptic CB1Rs (Kreitzer and Regehr, 2001; Diana et al., 2002; Szabo et al., 2004; Kawamura et al., 2006; Safo et al., 2006). *In vivo* administration of synthetic CB1R agonists in mice impairs cerebellum-dependent motor coordination (DeSanty and Dar, 2001; Patel and Hillard, 2001). Thus, the effects of CB1R agonists on cerebellar functions are well understood. Therefore, the cerebellum is the ideal neuronal circuit to examine the potency of synthetic cannabinoids, whose actions on neuronal functions have not been determined.

Here, using whole-cell patch-clamp recordings, we investigated activity of MAM-2201 in human CB1R (hCB1R)-expressing AtT-20 cells, and then the effects of MAM-2201 on synaptic transmission in slice preparations of the mouse cerebellum. We found that MAM-2201 acted as an agonist of hCB1Rs and inhibited excitatory transmitter release at PF-PC synapses via activation of presynaptic CB1Rs. MAM-2201 decreased the synaptic transmission more strongly than Δ^9-THC within the range of 0.1–30 μM and naphthalen-1-yl-(1-pentylindol-3-yl)methanone [JWH-018, Fig. 1*B*, one of the most popular and potent synthetic cannabinoids detected in the herbal products (Atwood et al., 2010)], within the range of 0.03–3 μM. Furthermore, MAM-2201 induced presynaptic suppression of CF-PC synapses, leading to a reduction in the number of spikelets in complex spikes and to attenuated dendritic Ca^{2+} transients in PCs.

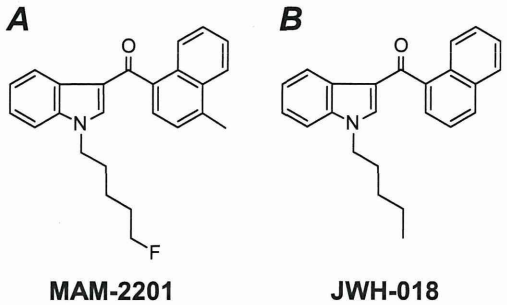

Fig. 1. The chemical structures of [1-(5-fluoropentyl)-1*H*-indol-3-yl](4-methyl-1-naphthalenyl)-methanone (MAM-2201, *A*) and naphthalen-1-yl-(1-pentylindol-3-yl) methanone (JWH-018, B).

2. Materials and methods

2.1. Cannabinoid-related compounds

MAM-2201 (Fig. 1*A*) and JWH-018 (Fig. 1*B*) were purchased from Cayman Chemical (Ann Arbor, MI, USA). (*R*)-(+)-[2,3-Dihydro-5-methyl-3-(4-morpholinylmethyl)pyrrolo[1,2,3-de]-1,4-benzoxazin-6-yl]-1-naphthalenylmethanone mesylate [WIN55,212-2 (WIN), a CB1R and CB2R agonist] and *N*-(Piperidin-1-yl)-5-(4-iodophenyl)-1-(2,4-dichlorophenyl)-4-methyl-1*H*-pyrazole-3-carboxamide (AM251, a CB1R antagonist) were purchased from Wako Pure Chemical Industries (Osaka, Japan) and Tocris Bioscience (Bristol, UK), respectively. Δ^9-THC was purchased from Cerilliant (Round Rock, TX, USA). These compounds were dissolved in dimethylsulfoxide as stock solutions. In electrophysiological recordings from AtT-20 cells and from cerebellar PCs, the final concentrations of dimethylsulfoxide in extracellular solutions were maintained at 0.1 and 0.3% (v/v), respectively. WIN was used as a positive control, because WIN has been used in many studies to suppress neurotransmitter release at PF-, CF-, and interneuron-PC synapses via activation of presynaptic CB1Rs (Kreitzer and Regehr, 2001; Diana et al., 2002; Safo and Regehr, 2005; Kawamura et al., 2006).

2.2. Heterologous expression of CB1R in AtT-20 cells

AtT-20 cells were obtained from JCRB Cell Bank (Osaka, Japan) and were maintained in Ham's F-10 medium (GIBCO, Grand Island, NY) supplemented with 10% horse serum (GIBCO), 2.5% fetal bovine serum (GIBCO), and a mixture of penicillin and streptomycin solution (100 unit/mL and 100 mg/mL, respectively; GIBCO) in a 5% CO_2 incubator at 37 °C. The cells were plated onto grass coverslips coated with poly-D-lysine (Sigma–Aldrich, St Louis, MO) for gene transfection. hCB1R (SC111611; Origene, Rockville, MD; NCBI Reference Sequence: NM_016083.3) (Bruno et al., 2014) or mouse CB1R (mCB1R, MC206086; Origene; GenBank: BC079564.1) cDNAs, and green fluorescent protein (GFP) vector were cotransfected into the cells in a 9:1 M ratio using Lipofectamine LTX (Invitrogen, Carlsbad, CA) according to the manufacturer's instructions. Fluorescence of GFP was regarded as an indicator of transfected cells. Whole-cell patch-clamp recordings were made from the GFP-positive cells 20–48 h after transfection. The expression of CB1R proteins was confirmed by immunostaining with the combination of rabbit polyclonal anti-CB1R antibody (1:2000 dilution, CB1-Rb-Af380, Frontier Institute, Hokkaido, Japan) and AlexaFluor 568-conjugated goat anti-rabbit IgG secondary antibody (5 μg/mL, A-11011; Invitrogen) according to the methods described previously (Irie et al., 2014).

The immunofluorescence signal was observed under a confocal microscope (A1R; Nikon, Tokyo, Japan; Fig. 2A).

2.3. Electrophysiological recordings from AtT-20 cells

AtT-20 cells were transferred to a recording chamber and continuously perfused at 2 mL/min with high-K^+ extracellular solution containing (in mM): 87 NaCl, 60 KCl, 2 $CaCl_2$, 1 $MgCl_2$, 10 D-glucose, and 10 4-(2-hydroxyethyl)-1-piperazineethanesulfonic acid (HEPES) (pH adjusted to 7.4 with NaOH). The concentration of KCl was raised compared to normal extracellular solution to increase amplitudes of inwardly rectifier potassium currents (Mackie et al., 1995). All experiments were performed at 25 ± 1 °C. The cells were visualized by Nomarski optics and a near infrared-CCD camera (C3077-79; Hamamatsu Photonics, Hamamatsu, Japan) with a 40 × 0.8 NA numerical aperture water-immersion objective lens (Olympus, Tokyo, Japan) on an upright microscope (BX51WI; Olympus). GFP-positive cells were visualized and selected using epifluorescence optics (Olympus).

Patch pipettes were made from borosilicate glass capillaries (GC150F-100; Harvard Apparatus, Holliston, MA) and had a resistance of 3–5 MΩ when filled with a potassium gluconate-based internal solution containing (in mM): 125 K-gluconate, 10 KCl, 3 $MgCl_2$, 0.1 ethylene glycol tetraacetic acid (EGTA), 5 Na_2-ATP, 5 Na_2-phosphocreatine, 0.3 Na_2-GTP, and 10 HEPES (pH adjusted to 7.3 with KOH). Whole-cell patch-clamp recordings were performed from GFP-positive cells, and inward currents were evoked by applying voltage steps from a holding potential of −25 mV to −110 mV for 200 ms in voltage-clamp conditions. Membrane capacitance was calculated from the transient current evoked by applying a small voltage step (−5 mV, 20 ms duration) from a holding potential of −25 mV (Irie et al., 2006). Series resistance was compensated electronically by 70–90%, and the liquid junction potential (−5 mV) was corrected off-line.

Data were collected with Molecular Devices (Sunnyvale, CA) hardware and software (Multiclamp 700B, Digidata 1440A, Clampex 10.3) as described previously (Irie et al., 2014), and analyzed using Clampfit 10.3 software (Molecular Devices) and Igor Pro 6 software (Wavemetrics, Lake Oswego, OR) with the added import functionality provided by ReadPclamp XOP of the NeuroMatic software package (http://www.neuromatic.thinkrandom.com/). Representative current traces are shown after averaging four consecutive traces. To obtain inward current densities induced by MAM-2201 or WIN, the amplitudes of the current were normalized to membrane capacitances (picoamperes per picofarad, Fig. 2C). The densities were plotted as a function of the concentration and fit with the sigmoidal function, Y = Bottom + (Top − Bottom)/(1 + ⟦10⟧ ^(LogEC50 − X)*Hillslope]), using GraphPad Prism 5 (GraphPad Software, San Diego, CA).

2.4. Cerebellar slice preparation and electrophysiological recordings from PCs

ICR mice of either sex [postnatal day (P) 20–57 for Figs. 3–5 and Table 1; P14–20 for Figs. 6 and 7, and Table 2] were used according to the guidelines for animal use of the National Institute of Health Sciences. Cerebellar slices were prepared as described previously with some modifications (Shuvaev et al., 2011). Briefly, mice were anesthetized with halothane and decapitated. Parasagittal slices of the cerebellum (200-μm thick) were prepared using a microslicer (PRO7, Dosaka, Kyoto, Japan) in ice-cold, cutting solution containing (in mM): 234 sucrose, 2.5 KCl, 1.25 NaH_2PO_4, 10 $MgSO_4$, 0.5 $CaCl_2$, 26 $NaHCO_3$, 11 glucose, and bubbled with 5% CO_2/95% O_2. The slices were then allowed to recover for 1 h at room temperature in artificial cerebrospinal fluid (ACSF) solution containing (in mM): 120 NaCl, 2.5 KCl, 2 $CaCl_2$, 1 $MgCl_2$, 1.25 NaH_2PO_4, 26 $NaHCO_3$, 17 glucose, 0.4 ascorbic acid, 3 myo-inositol, 2 sodium pyruvate, and bubbled with 5% CO_2/95% O_2. In electrophysiological recordings, ascorbic acid, myo-inositol, and sodium pyruvate were omitted.

Cerebellar slices were transferred to a recording chamber, and continuously perfused at 2 mL/min with ACSF at 25 ± 1 °C (Figs. 3–6 and Table 1) or near physiological temperature (34 ± 1 °C; Fig. 7 and Table 2). Electrophysiological recordings were done using the same equipment described above. Excitatory and inhibitory postsynaptic currents (EPSCs and IPSCs) were recorded in the presence of 100 μM picrotoxin (a $GABA_A$ receptor antagonist, Tocris Bioscience) and 40 μM 6,7-dinitroquinoxaline-2,3-dione (DNQX, an AMPA/kainate receptor antagonist, Tocris Bioscience), respectively. Patch pipettes had a resistance of 2–3 MΩ when filled with pipette solutions. A CsCl-based and the K-gluconate-based internal solutions were used for voltage- (Figs. 3–6 and Table 1) and current-clamp recordings (Fig. 7 and Table 2), respectively. The CsCl-based solution contained (in mM): 120 CsCl, 20 K-gluconate, 15 tetraethylammonium-Cl, 3 $MgCl_2$, 5 EGTA, 5 Na_2-ATP, 5 Na_2-phosphocreatine, 0.3 Na_2-GTP, 5 QX-314, and 10 HEPES (pH adjusted to 7.3 with CsOH). The liquid junction potentials (CsCl-based, −4 mV; K-gluconate-based, −10 mV) were corrected off-line.

Somatic whole-cell patch-clamp recordings were performed from PCs in lobules IV to VIII. PF-PC EPSCs and IPSCs were evoked by electrical stimulation of the molecular layer and recorded at the holding potential of −80 mV. CF-PC EPSCs and complex spikes were evoked by the stimulation of the granule cell layer. CF-PC EPSCs were recorded at a holding potential of −10 mV to decrease the driving force for cations through ionotropic glutamate receptors. The stimuli (100- to 200-μs pulses, 20–80 V amplitude) were performed with an ACSF-filled patch pipette (tip diameter, 10–15 μm for molecular layer stimulation and 2–3 μm for the granule cell layer) and applied at 0.1 Hz. In some experiments, paired-pulse stimulation (50 ms inter-stimulus intervals) was done to calculate the paired-pulse ratio (PPR), which is an index of the change of neurotransmitter release from presynaptic terminals (Zucker and Regehr, 2002; Irie and Ohmori, 2008). When postsynaptic currents were recorded, series resistance was monitored by applying small voltage steps (−10 mV, 20-ms duration), and the records were discarded if the resistance varied more than 25%. Quantal EPSCs (qEPSCs) from PFs and CFs were elicited by electrical stimulation (0.1 Hz) with PCs held at −80 mV and with $CaCl_2$ in ACSF replaced with equimolar $SrCl_2$ (Xu-Friedman and Regehr, 1999). Miniature IPSCs (mIPSCs) were recorded at a holding potential of −80 mV in the presence of 40 μM DNQX and 1 μM tetrodotoxin (TTX; Wako Pure Chemical Industries). In the start of current-clamp recordings, resting membrane potentials of PCs were adjusted at −60 to −70 mV by current injection to prevent spontaneous firing, and series resistance was compensated for using bridge balance and capacitance neutralization. Intrinsic membrane properties were examined by square-wave current injection (500-ms duration, Table 2). Input resistance was measured from averaged voltage responses evoked by small hyperpolarizing currents (−20 pA). Threshold current and threshold potential were measured by depolarizing current injections (from 0 pA to 200 pA, 20 pA increment). The maximum rate of rise and maximum rate of fall of action potentials and spike height were calculated from the first action potential waveform evoked at the threshold current. Firing frequency was obtained from the number of spikes observed during the current injection.

qEPSCs and mIPSCs were detected off-line using the template search function in the Clampfit 10.3 software. To analyze qEPSCs, data from 200 to 1600 ms after the stimulus artifact were used. Average cumulative probability histograms were obtained as follows: first, qEPSCs or mIPSCs were recorded more than 300 events from each cell in the presence or absence of MAM-2201. Then, for each cell, the amplitudes and inter-event intervals were binned, and individual cumulative probability histograms were plotted. Finally, these histograms were averaged. Representative EPSC and IPSC traces are shown after averaging four to six consecutive traces, and stimulus artifacts are truncated. EPSC and IPSC amplitudes were obtained by averaging six consecutive records. The coefficient of variation (CV), which is another index of the change of neurotransmitter release from presynaptic terminals, was calculated from 18 consecutive EPSC or IPSC traces (Korn and Faber, 1991). The inhibitory concentration 50% (IC50) values of the cannabinoid-related compounds against neurotransmitter release at PF-PC synapses were calculated as follows: control PF-PC EPSC amplitude was obtained from the averaged EPSCs recorded for 3 min before application of the synthetic cannabinoids. PF-PC EPSC amplitude in the presence of the cannabinoids was done from the EPCSs recorded for 8 to 10 min after the application, normalized to the control values, and plotted as a function of the concentration. The data were fit with the sigmoidal function, Y = 100/(1 + ⟦10⟧ ^(LogIC50 − X)*Hillslope]) (Table 1). The reasons for using PF-PC synapses for measurement of IC50s were as follows: PF-PC synapses exhibit more stable synaptic transmission than interneuron-PC synapses (Vincent and Marty, 1996), they are more sensitive to CB1R agonists, and they express CB1R proteins more abundantly than CF-PC synapses (Kawamura et al., 2006).

2.5. Simultaneous recordings of Ca^{2+} transients and complex spikes

Current-clamp recordings were done from PCs using the K-gluconate-based intracellular solution in which EGTA was replaced with 100 μM Oregon Green 488 BAPTA-1 hexapotassium salt (OGB-1; Invitrogen, Carlsbad, CA) in the presence of picrotoxin. PC somata and dendrites were dialyzed with the pipette solution for 30 min to obtain a stable intracellular concentration of OGB-1. Confocal imaging was then performed with a Nipkow disk confocal scanner unit (CSU-10; Yokogawa Electric, Tokyo, Japan) attached to the Olympus BX51WI microscope with the 40× objective lens. A 488 nm beam from a diode laser (Yokogawa Electric) for excitation was coupled to the scanner unit through an optical fiber. Fluorescence was detected via a 520 nm long-path filter using an EMCCD camera (iXon3 DU897; Andor Technology, Belfast, Northern Ireland). The pixels were binned 2 × 2 on the chip, and images were acquired at 25.8 Hz. Complex spikes were evoked at 0.1 Hz, and the electrophysiological recordings were synchronized with the acquisition of time-lapse fluorescent images. The number of spikelets in complex spikes was obtained from average value of five to seven consecutive traces. The imaging experiments were controlled and analyzed using Andor iQ2 software (Andor Technology). Three to five consecutive time-lapse images were averaged and used for analysis. The regions of interests were set on primary dendrites (approximately between 20 and 100 μm from the center of the cell body, Fig. 7Ca). Fluorescence changes were background-corrected and expressed as $\Delta F/F_0$, where F_0 is the fluorescence intensity when the cells were at rest, and ΔF is the absolute values of fluorescence changes during activity. Integration of Ca^{2+} transients was performed over 2 s from the onset.

All data other than EC50s or IC50s are provided as the means ± standard deviation. EC50s and IC50s are expressed as the best-fit values with 95% confidence interval (CI; Table 1). *n* indicates the number of experiments. Statistical significance was tested using paired *t*-tests test unless otherwise stated (significance, $p < 0.05$).

3. Results

3.1. MAM-2201 acts as an agonist of hCB1Rs and mCB1Rs

To examine whether MAM-2201 activates CB1Rs, we expressed hCB1R or mCB1R cDNAs in murine tumor line AtT-20. Because

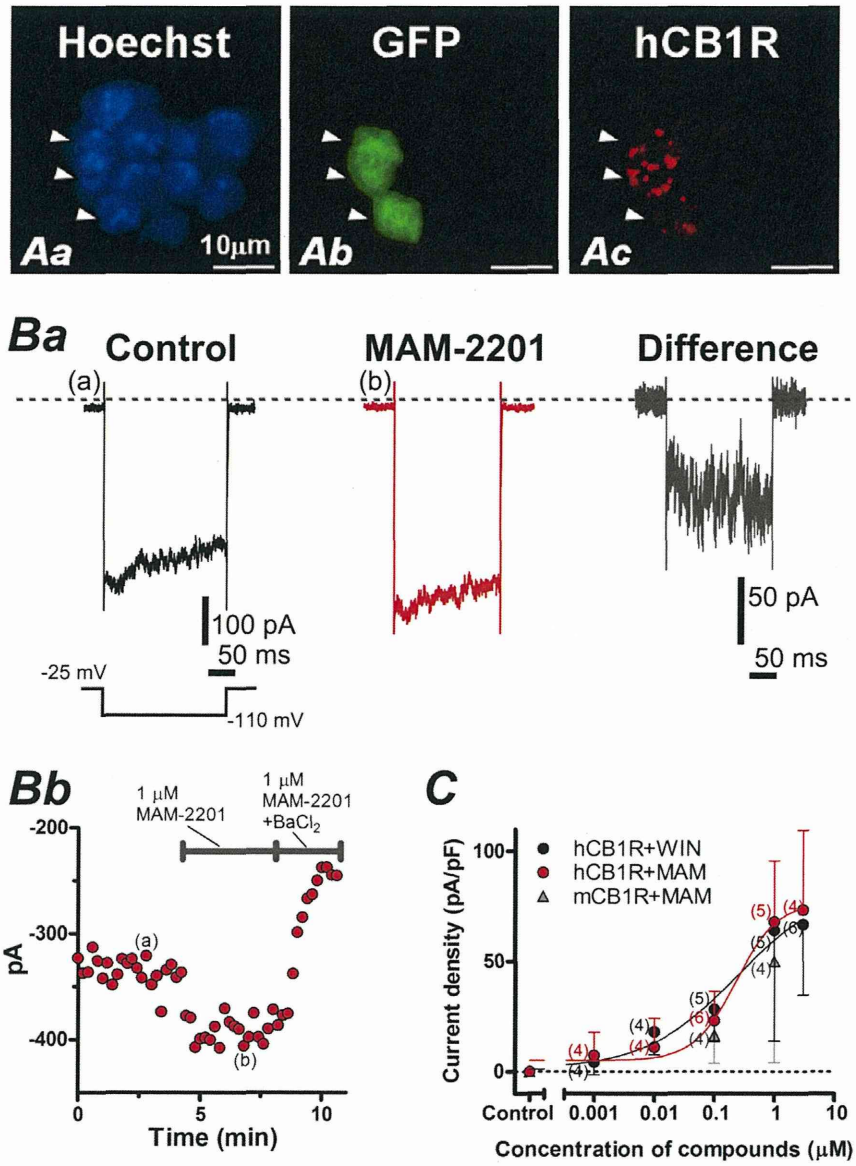

Fig. 2. Heterologous expression of cannabinoid receptor type 1 (CB1R) cDNAs in AtT-20 cells. A, Immunofluorescence images of AtT-20 cells transfected with human CB1R (hCB1R) and green fluorescent protein (GFP) cDNAs. Cell nuclei were stained with Hoechst 33342 (1 μg/mL, Dojindo, Kumamoto, Japan; Aa). Arrowheads indicate GFP and hCB1R double positive cells. Proteins of hCB1Rs were visualized by immunolabelling with rabbit anti-CB1R antibody and AlexaFluor 568-conjugated anti-rabbit secondary antibody (Ac). B, Representative data recorded from hCB1R-expressing cell. Ba, Inward currents were evoked by applying voltage steps from a holding potential of −25 mV to −110 mV for 200 ms. In trace (a) and (b), averages of four consecutive responses are shown. These traces correspond to the responses at time points marked (a) or (b) in Bb. The holding current level is shown by a dotted line. Bb, Time course of mean inward currents. Each point represents an averaged value obtained from four consecutive records. C, Concentration-dependent increases of inward current densities induced by MAM-2201 or (*R*)-(+)-[2,3-Dihydro-5-methyl-3-(4-morpholinylmethyl)pyrrolo[1,2,3-de]-1,4-benzoxazin-6-yl]-1-naphthalenylmethanone mesylate [WIN55,212-2 (WIN)]. To obtain current densities, amplitudes of inward current induced by MAM-2201 or WIN were normalized to membrane capacitances (picoamperes per picofarad). The densities were plotted as a function of the concentration and fit with the sigmoidal function, $Y = \text{Bottom} + (\text{Top} - \text{Bottom})/(1 + 〚10〛^{[(\text{LogEC50} - X)*\text{Hillslope}]})$, where EC50 is effective concentration 50%. Here and in the following figures, error bars and the numbers in parentheses indicate standard deviation and the number of experiments, respectively.

application of CB1 agonists on AtT-20 cells expressing CB1Rs activates inward rectifier potassium currents, activities of compounds against CB1Rs can be determined using this heterologous expression system (Mackie et al., 1995; Felder et al., 1998). Whole-cell patch clamp recordings were done from hCB1R or mCB1R-expressing cells, and inward currents were evoked by applying hyperpolarizing voltage pulses (Fig. 2*B*). Bath application of MAM-2201(1 μM) increased the amplitude of inward current within 5 min (Fig. 2*Bb*). Subsequent application of low concentration of Ba^{2+} (200 μM $BaCl_2$), which blocks inward rectifier potassium currents (Hagiwara et al., 1976), markedly reduced the inward currents. This indicates that, in addition to MAM-2201-induced currents, MAM-2201-independent inward rectifier potassium currents were simultaneously blocked (Dousmanis and Pennefather, 1992). The time course of the induced current, obtained by subtracting the currents before from those after the application of MAM-2201, showed slow activation at the beginning of voltage pulse (Fig. 2*Ba*, Difference). This property is characteristic of activation of G-protein coupled potassium channels (Kubo et al., 1993). Fig. 2*C* shows the concentration-dependent increase of current

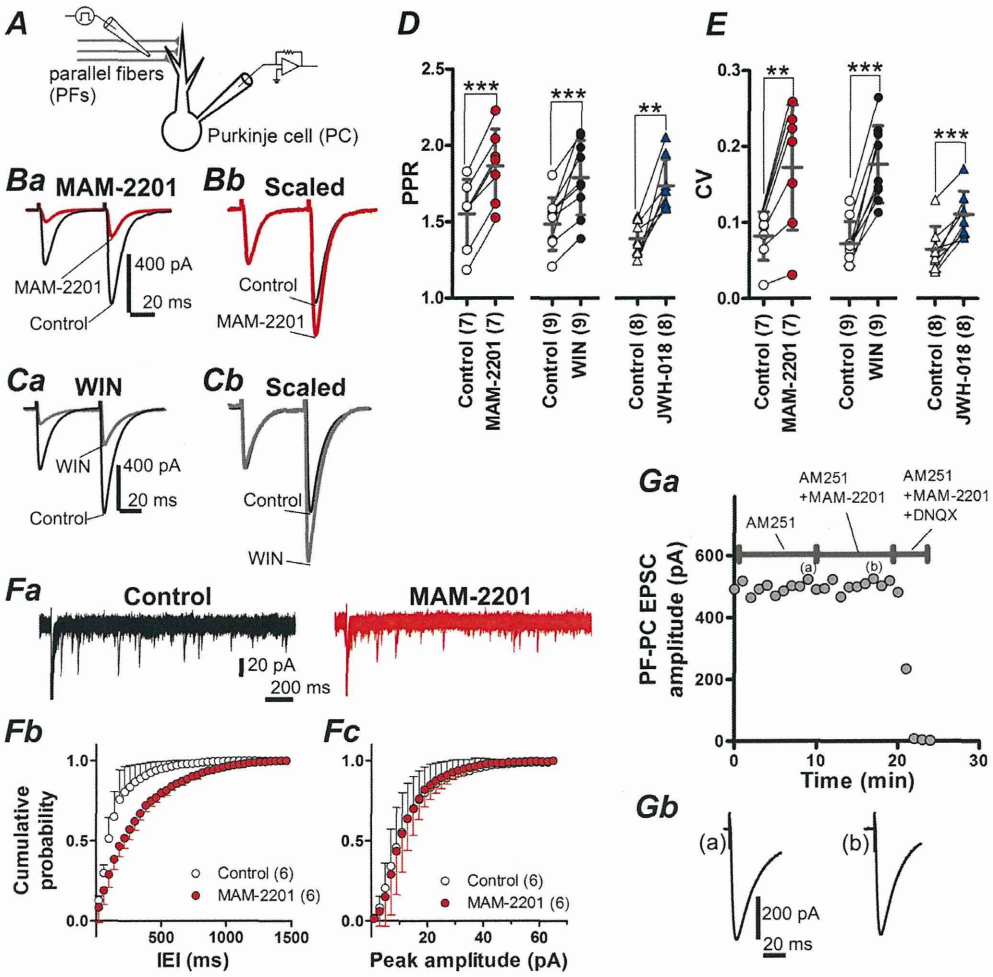

Fig. 3. MAM-2201 inhibits synaptic transmission at parallel fiber (PF)-Purkinje cell (PC) synapses presynaptically via activation of presynaptic CB1Rs. *A*, Experimental configuration for Fig. 3*B–G* and 4. *B*, PF-induced excitatory postsynaptic currents (EPSCs) were evoked with pairs of stimuli (50 ms interval) under control conditions (Control) or in the presence of 10 μM MAM-2201 (MAM-2201). The holding potential was −80 mV. Picrotoxin (100 μM) was added to the extracellular artificial cerebrospinal fluid (ACSF) to block $GABA_A$ receptor-mediated inhibitory postsynaptic currents (IPSCs). The first EPSC peak in MAM-2201 was reduced to 21.9% of control. In each trace, averages of six trials are shown. In the right panel, the EPSC evoked by the first stimulus in MAM-2201 is scaled to the amplitude of the first EPSC in Control. MAM-2201 increased paired-pulse facilitation (*Bb*). Stimulus artifacts are truncated. *C*, Same as in *A*, but in the presence of 10 μM WIN. In *Ca*, the first peak in WIN was reduced to 24.1% of control. In the right panel, the EPSC evoked by the first stimulus in WIN is scaled to the amplitude of the first EPSC in Control. *D* and *E*, Summary of paired-pulse ratio (PPR, *D*) and coefficient of variation (CV, *E*) of PF-PC EPSCs before and after application of MAM-2201, WIN, or JWH-018 (10 μM in all groups). Here and in the following figures, the statistical significance was tested using paired *t*-tests unless otherwise stated (significance, $p < 0.05$). $^{**}p < 0.01$ and $^{***}p < 0.001$. *F*, To isolate quantal EPSCs (qEPSCs) from PFs, asynchronous neurotransmitter release from PF terminals was evoked by stimulating PFs in the presence of Sr^{2+} (2 mM, see Materials and Methods). *Fa*, Five superimposed traces before (Control) and after application of MAM-2201. Asynchronously released quanta are seen as downward current deflections. Synchronous PF-PC EPSCs are truncated. *Fb* and *Fc*, Average cumulative probability histograms of inter-event interval (IEI, *Eb*, bin width: 40 ms) and peak amplitude (*Ec*, bin width: 2 pA) of PF-PC qEPSCs. *Ga*, Time course of peak PF-PC EPSC amplitudes in the presence of *N*-(Piperidin-1-yl)-5-(4-iodophenyl)-1-(2,4-dichlorophenyl)-4-methyl-1*H*-pyrazole-3-carboxamide (AM251, 5 μM). Each point represents an averaged value obtained from six consecutive records. MAM-2201 (10 μM) had no detectable effect on the amplitude. Additional application of 6,7-dinitroquinoxaline-2,3-dione (DNQX, 40 μM) abolished PF-PC EPSCs completely. *Gb*, Traces show normalized PF-PC EPSC responses at time points marked (a) and (b) in *Ga*.

densities induced by MAM-2201 or WIN in CB1R-expressing cells. Interestingly, in hCB1R-expressing cells, MAM-2201 increased current densities in a concentration-dependent manner (Fig. 2*C*, red circles) with an EC50 of 0.230 μM (95% CI, 0.0384–1.37 μM). Similar responses were obtained by application of WIN (Fig. 2*C*, black circles; EC50 = 0.234 μM; 95% CI, 0.410 × 10^{-3}-140 μM), which was consistent with previous report (Mackie et al., 1995). In the presence of AM251 (5 μM, a CB1R antagonist), MAM-2201 (1 μM) did not induce the inward currents (−2.38 ± 7.23 pA/pF, $n = 6$). In cells transfected with GFP alone, MAM-2201 (1 μM) did not elicit any changes (1.55 ± 6.78 pA/pF, $n = 5$). In mCB1R-expressing cells, MAM-2201 induced concentration-dependent increase in the current density (Fig. 2*C*, gray triangles). These results demonstrate that MAM-2201 activates hCB1Rs and mCB1Rs.

3.2. MAM-2201 inhibits synaptic transmission presynaptically via activation of presynaptic CB1Rs at PF-PC synapses in mouse cerebellum

We tested the effects of MAM-2201 on neurotransmitter release at PF-PC synapses and the involvement of CB1Rs (Fig. 3), and compared the potency of MAM-2201 with that of WIN, JWH-018, and Δ^9-THC (Fig. 4 and Table 1). Whole-cell patch-clamp recordings were performed from somata of PCs in mouse cerebellar slices under voltage-clamp conditions, and PF-PC EPSCs were evoked by electrical stimulation of PFs in the molecular layer in the presence of picrotoxin. The recording configuration is illustrated in Fig. 3*A*. As shown in Fig. 3*B*, bath application of MAM-2201 (10 μM, 8 min) significantly decreased the first EPSC amplitude

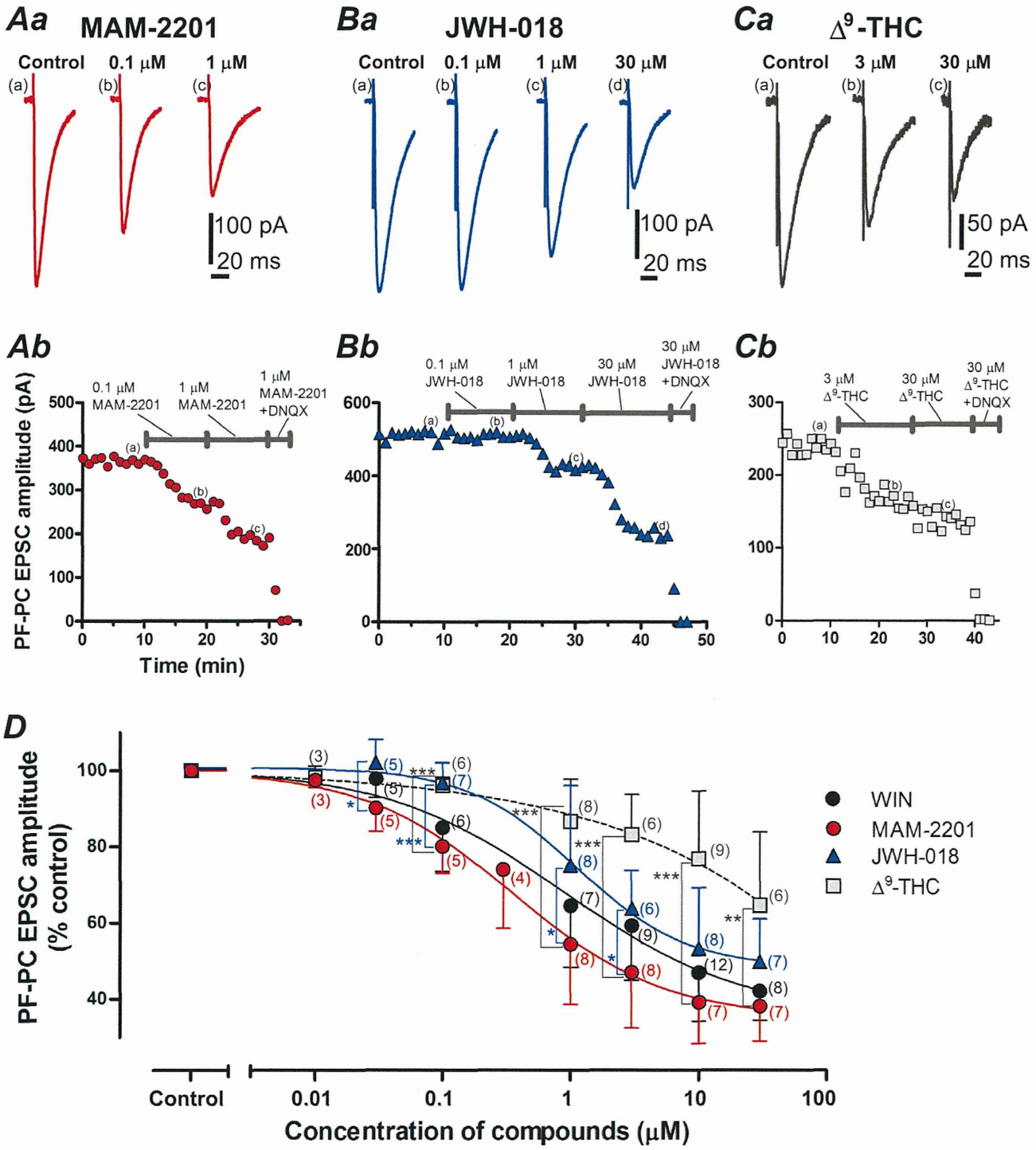

Fig. 4. MAM-2201 is a more potent inhibitor than Δ^9-tetrahydrocannabinol (Δ^9-THC) and JWH-018 at PF-PC synapses. *Aa*, Representative PF-PC EPSC traces recorded in control conditions, or in 0.1 or 1 μM MAM-2201. These traces show normalized PF-PC EPSC responses at time points marked (a), (b), or (c) in *Ab*. *Ab*, Time course of peak amplitudes of PF-PC EPSCs. Each point represents an averaged value obtained from six consecutive records. *Ba*, Representative PF-PC EPSC traces recorded in control conditions, or in 0.1, 1, or 30 μM JWH-018. These traces correspond to the responses at time points marked (a), (b), (c), or (d) in *Bb*. *Bb*, Time course of peak amplitudes of PF-PC EPSCs. *C*, Representative PF-PC EPSC traces recorded in control conditions, or in 3, or 30 μM Δ^9-THC. These traces correspond to the responses at time points marked (a), (b), or (c) in *Cb*. *Cb*, Time course of the peak amplitudes. In *Aa*, *Ba*, and *Ca*, stimulus artifacts are truncated. *D*, Concentration-dependent decreases of PF-PC EPSC amplitudes induced by cannabinoid-related compounds. Control PF-PC EPSC amplitude was obtained from averaged PF-PC EPSCs recorded for 3 min before the application of the compounds. PF-PC EPSC amplitudes in the presence of these compounds were recorded for 8–10 min after application, normalized to the control values, and plotted as a function of concentration (Fig. 4C). Each plot was fit with a sigmoidal function, $Y = 100/(1 + [10]^{[(LogIC50 - X)*Hillslope]})$, where IC50 is inhibitory concentration 50%. $^*p < 0.05$, $^{**}p < 0.01$, and $^{***}p < 0.001$ by unpaired *t*-tests test.

(39.0 ± 10.8% of control value, $n = 7$, $p < 0.001$). To investigate whether the effects of MAM-2201 on PF-PC EPSC amplitude were mediated by presynaptic mechanisms, PPR and CV analyses were performed. MAM-2201 (10 μM) significantly increased PPR (Fig. 3*Bb* and *D*) and CV (Fig. 3*E*), indicating a decrease in presynaptic neurotransmitter release. WIN (10 μM, 8-min application) induced a similar decrease in PF-PC EPSC amplitude and a parallel increase in the PPR and CV (Fig. 3*C–E*). MAM-2201 (10 μM) also

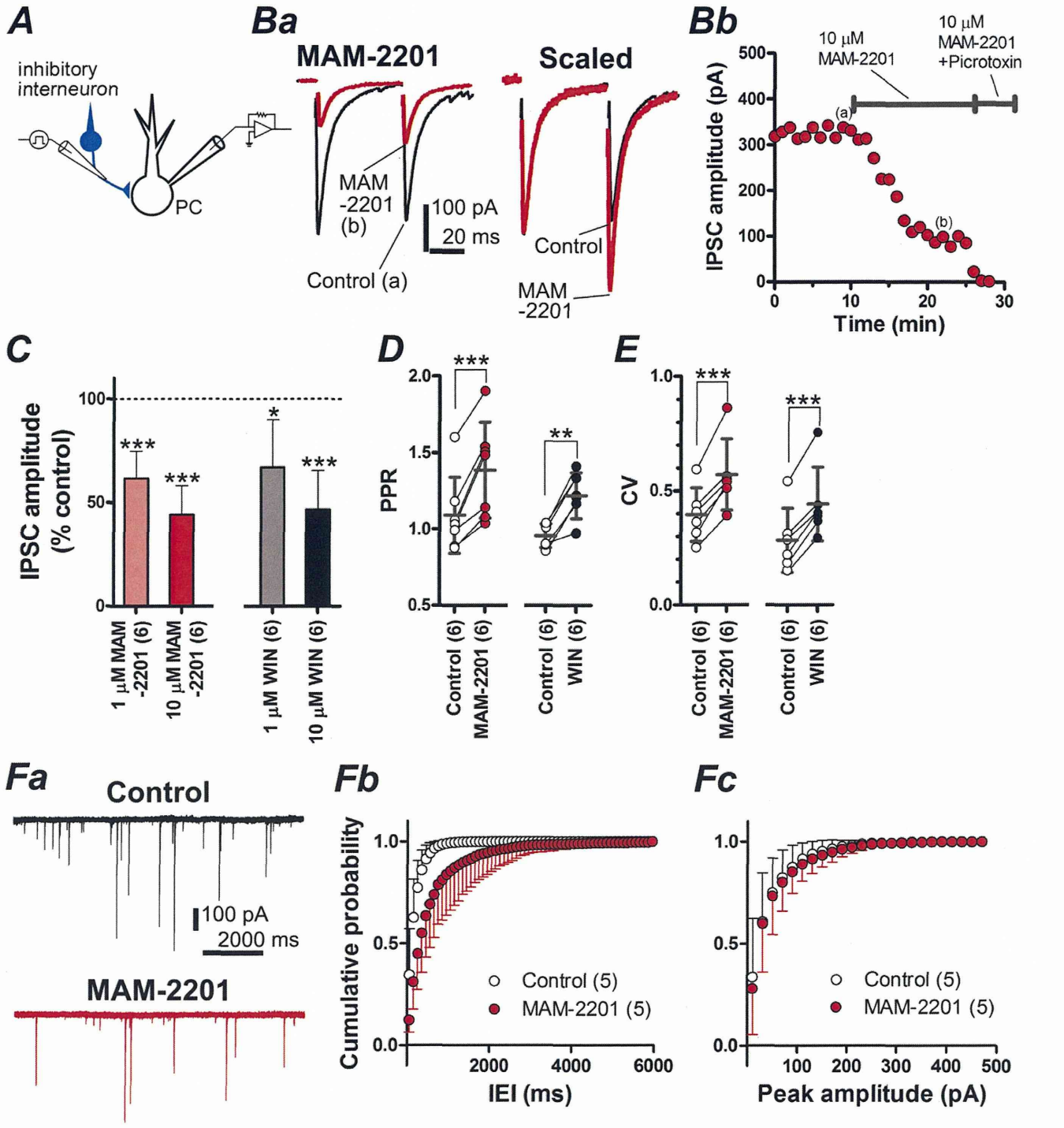

Fig. 5. MAM-2201 reduces GABAergic synaptic transmission at interneuron-PC synapses via presynaptic mechanisms. *A*, Experimental configuration for Fig. 5*B–E*. *Ba*, Averaged current traces of IPSCs in control conditions (Control) and 10 μM MAM-2201. These traces show normalized IPSC responses at time points marked (a) and (b) in *Bb*. IPSCs were evoked with pairs of stimuli (50 ms interval) in the presence of 40 μM DNQX and were recorded as inward currents because of the use of the CsCl-based internal solution. The holding potential was −80 mV, and stimulus artifacts were blanked for clarity. The first peak in MAM-2201 was reduced to 28.0% of control. In the right panel, the first IPSC in MAM-2201 is scaled to the amplitude of the first IPSC in Control (Scaled), showing a clear increase of PPR. *Bb*, Time course of peak amplitudes of the first IPSC. Each point represents an averaged value obtained from six consecutive records. *C*, Concentration-dependent decreases of peak amplitude of IPSC by MAM-2201 and WIN. IPSC amplitudes were normalized to the control value (=baseline responses) and expressed as a percentage of control. $*p < 0.05$ and $***p < 0.001$. *D* and *E*, Summary of PPR (*D*) and CV (*E*) of IPSCs before and after application of MAM-2201 and WIN (10 μM in both groups). $**p < 0.01$. *F*, Miniature IPSCs (mIPSCs) recorded in the presence of tetrodotoxin (TTX, 1 μM) and DNQX. *Fa*, Five superimposed traces before (Control) and after application of MAM-2201. mIPSCs appear as downward current deflections. *Fb* and *Fc*, Average cumulative probability histograms of IEI (*Fb*, bin width: 100 ms) and peak amplitude (*Fc*, bin width: 20 pA) of mIPSCs.

decreased PF-PC qEPSC frequency [Inter-event interval (IEI), Control: 194.0 ± 24.1 ms, MAM-2201: 288.7 ± 30.2 ms, $p < 0.001$, $n = 6$, Fig. 3*Fa* and *Fb*] without affecting PF-PC qEPSC amplitude (peak amplitude, Control: 18.9 ± 2.1 pA, MAM-2201: 18.6 ± 4.3 pA, $p = 0.860$, $n = 6$, Fig. 3*Fa* and *Fc*). In the absence of MAM-2201, amplitudes of PF-PC EPSCs did not show significant changes during 45-min recording under condition in which series resistance was stable (105.2 ± 10.5% of control, $n = 7$, $p = 0.271$).

Table 1
IC50s of synthetic cannabinoids against PF-PC EPSCs.

	WIN	MAM-2201	JWH-018
IC50 (μM) [95% CI (μM)][a]	0.890 [0.296-2.679]	0.363 [0.193-0.681]	1.121 [0.551-2.282]
Relative IC50	1.00	0.41	1.25

[a] Data are provided as the best-fit values with 95% confidence intervals (CI).

To examine whether MAM-2201 altered postsynaptic responses by activating presynaptic CB1Rs, MAM-2201 was bath-applied to the cerebellar slices in the presence of AM251 (5 μM). MAM-2201 did not induce any change of PF-PC EPSC amplitude in the presence of AM251 (Fig. 3G, 102.2 ± 6.0% of control, $n = 5$, $p = 0.443$). Subsequent application of DNQX (40 μM) abolished PF-PC EPSCs, demonstrating that glutamatergic synaptic transmission was indeed evoked, and bath application of these chemicals was successful (Fig. 3Ga). Taken together, these results indicate that the MAM-2201-induced changes are mediated by a decrease in presynaptic neurotransmitter release from PF terminals via activation of presynaptic CB1Rs.

3.3. MAM-2201 is a more potent inhibitor of PF-PC synapses than Δ^9-THC and JWH-018

Fig. 4A–C show representative traces of PF-PC EPSCs in the presence of MAM-2201 (Fig. 4A), JWH-018 (Fig. 4B), or Δ^9-THC (Fig. 4C), respectively. The inhibitory effect of MAM-2201 on PF-PC

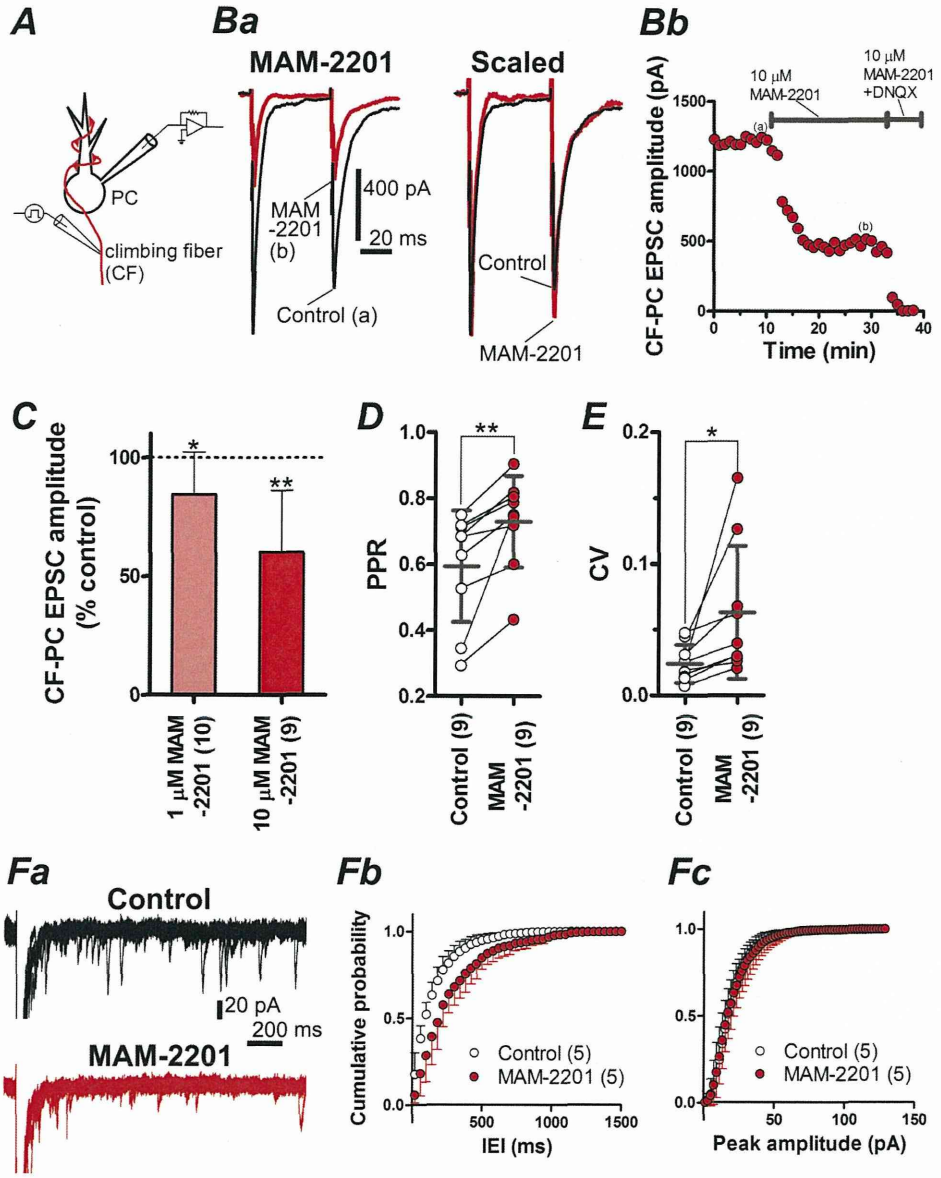

Fig. 6. MAM-2201-mediated presynaptic inhibition at climbing fiber (CF)-PC synapses. *A*, Experimental configuration for Fig. 6*B–F* and 7. *Ba*, Averaged current traces of CF-PC EPSCs in control (Control) and 10 μM MAM-2201. These traces show normalized CF-PC EPSC responses at time points marked (a) and (b) in *Bb*. CF-PC EPSCs were evoked with pairs of stimuli (50 ms interval) in the presence of 100 μM picrotoxin. PCs were held at −10 mV to reduce the driving force for AMPA receptor-mediated currents. Stimulus artifacts were truncated for clarity. The first peak in MAM-2201 was reduced to 38.4% of control. In the right panel, the first CF-PC EPSC in MAM-2201 is scaled to the amplitude of the first CF-PC EPSC of control (Scaled). *Bb*, Time course of peak amplitudes of first CF-PC EPSC. Each point represents an averaged value obtained from six consecutive records. *C*, Concentration-dependent decreases of the peak amplitudes of CF-PC EPSCs by MAM-2201. CF-PC EPSC amplitudes were expressed as a percentage of control. *$p < 0.05$ and **$p < 0.001$. *D* and *E*, Summary of PPR (*D*) and CV (*E*) of CF-PC EPSCs before and after application of MAM-2201 (10 μM). *F*, CF-PC qEPSCs in the presence of picrotoxin and Sr^{2+} (2 mM $SrCl_2$). The qEPSCs were recorded at a holding potential of −80 mV. *Fa*, Five superimposed traces before (Control) and after application of MAM-2201. Synchronous CF-PC EPSCs are truncated. *Fb* and *Fc*, Average cumulative probability histograms of IEI (*Fb*, bin width: 40 ms) and peak amplitude (*Fc*, bin width: 2 pA) of CF-PC qEPSCs.

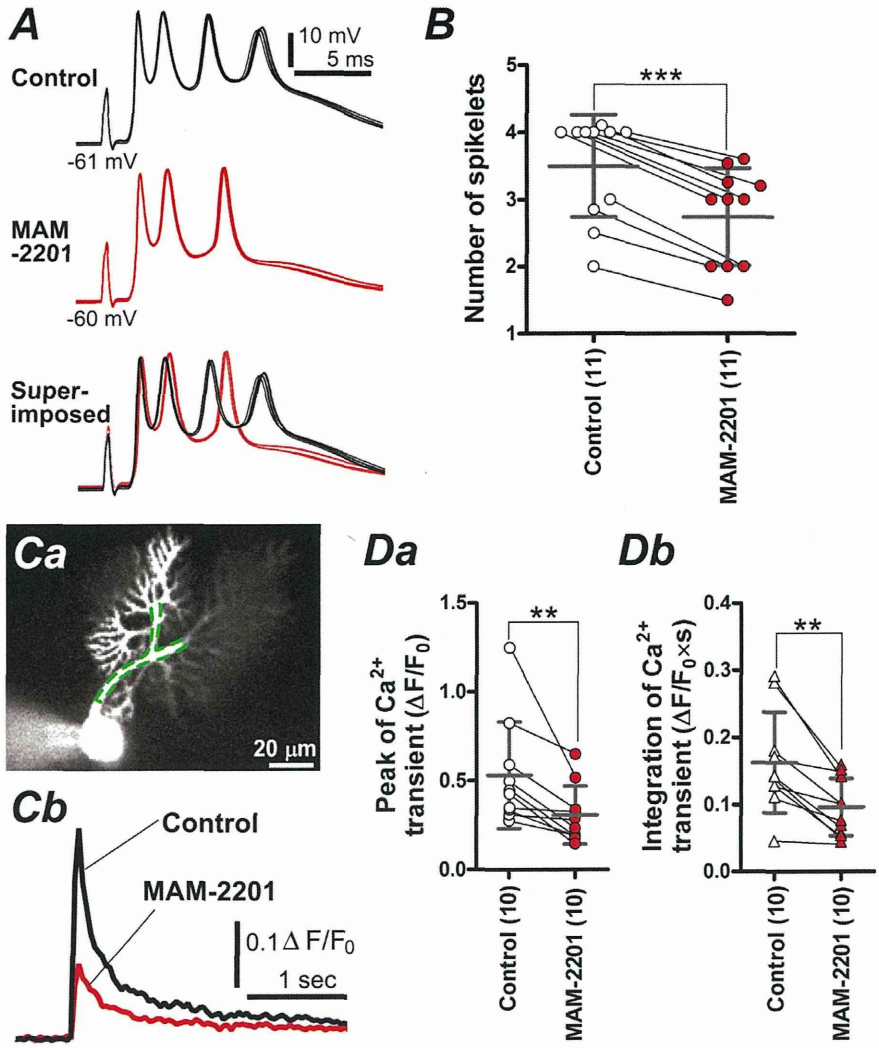

Fig. 7. MAM-2201 reduces the number of spikelets in complex spikes and dendritic Ca^{2+} transients evoked by CF stimulation. *A–D*, Simultaneous recordings of complex spikes and dendritic Ca^{2+} transients. *A*, Representative superimposed traces of complex spikes (5 traces) evoked by stimulation of CFs (0.1 Hz) in the presence of picrotoxin at near physiological temperature (34 ± 1 °C). The K-gluconate-based intracellular solution containing Oregon Green 488 BAPTA-1 hexapotassium salt (OGB-1, 100 μM) was used for current-clamp recordings. At the start of the recording, the resting membrane potential was adjusted around −60 to −70 mV by current injection to prevent spontaneous firing. MAM-2201 (10 μM, 10 min) reduced the number of spikelets (4 spikelets in Control; 3 spikelets in MAM-2201). Superimposed traces reveal delay and reduction of spikelets in MAM-2201. *B*, Summary of average number of spikelets before and after application of MAM-2201 (10 μM). ***$p < 0.001$. *C*, A dendritic Ca^{2+} transient induced by CF stimulation. Intracellular Ca^{2+} measurement in *C* was simultaneously performed while recording the complex spikes in *A*. *Ca*, Representative confocal image of PC loaded with OGB-1 via a patch pipette. Area indicated by dotted line represents region of interest used for the calculation of the dendritic Ca^{2+} transients. *Cb*, Representative Ca^{2+} transients in control and MAM-2201 (10 μM). F_0 is the fluorescence intensity when the cells were at rest, and ΔF is the absolute values of fluorescence changes during activity. *Da* and *Db*, Summary of Ca^{2+} transient peaks (*Da*) and integration of Ca^{2+} transients (*Db*). The integration was performed for 2 s from the onset. **$p < 0.01$.

EPSC amplitude was first detectable at 0.03 μM (Fig. 4*D*, 90.1 ± 6.1% of control, $n = 5$, $p < 0.05$), and became more apparent at higher concentrations. Application of 0.1 μM MAM-2201 was sufficient to induce a clear reduction [trace (b) in Fig. 4*Aa*, 71.9% of control], and subsequent administration of 1 μM MAM-2201 induced further decrease [trace (c) in Fig. 4*Aa*, 51.0% of control]. On the other hand, 0.1 μM JWH-018 did not have detectable effects on PF-PC EPSCs [trace (b) in Fig. 4*Ba*, 99.0% of control; 0.1 μM JWH-018 in Fig. 4*D*, $n = 7$, $p = 0.096$]. Higher concentrations of JWH-018 were required to reduce PF-PC EPSC amplitude [trace (c) in Fig. 4*Ba*, 1 μM, 81.0% of control; trace (d) in Fig. 4*Ba*, 30 μM, 44.2% of control]. Application of Δ^9-THC, which acts as a partial agonist of CB1Rs (Shen and Thayer, 1999; Luk et al., 2004), decreased amplitude of PF-EPSCs obviously at 3 μM [trace (b) in Fig. 4*C*, 68.6% of control], but subsequent administration of 30 μM Δ^9-THC did not induce a clear reduction [trace (c) in Fig. 4*C*, 57.0% of control]. Δ^9-THC (30 μM) significantly increased PPR and CV ($n = 6$, data not shown), indicating a decrease in presynaptic neurotransmitter release. Fig. 4*D* shows the concentration-dependent decreases of PF-PC EPSC amplitude induced by cannabinoid-related compounds. MAM-2201 decreased PF-PC EPSCs more potently than JWH-018 within the range of 0.03–3 μM (Fig. 4*D*, blue triangles (in the web version), $p < 0.05$ and $p < 0.01$ by unpaired *t*-tests test) and Δ^9-THC within the range of 0.1–30 μM (Fig. 4*D*, gray squares, $p < 0.001$ by unpaired *t*-tests test). Application of WIN decreased PF-PC EPSC amplitude to 64.5 ± 0.16% ($n = 7$) of the control value at a concentration of 1 μM and to 46.8 ± 0.13% ($n = 12$) at 10 μM (Fig. 4*D*, WIN). These results are comparable to the previous reports using cerebellar slice preparations from rodents (see Discussion) (Levenes et al., 1998; Takahashi and Linden, 2000; Kawamura et al., 2006). The IC50s of the synthetic cannabinoids against PF-PC EPSCs are summarized in Table 1, and indicate that the rank order of potency for inhibition is MAM-

Table 2
MAM-2201 did not affect intrinsic membrane properties of PCs.

	Control ($n = 10$)	10 μM MAM-2201 ($n = 10$)	p value
Resting membrane potential (mV)	−65.3 ± 3.2	−66.0 ± 3.5	0.43
input resistance (MΩ)	113 ± 51	101 ± 34	0.29
Threshold current (pA)	71.0 ± 39.5	77.8 ± 7.4	0.24
Threshold potential (mV)	−45.4 ± 5.6	−44.9 ± 6.4	0.50
Spike height (mV)	44.9 ± 6.4	45.4 ± 47.6	0.71
Maximum rate of rise (V/s)	114 ± 40	131 ± 37	0.20
Maximum rate of fall (V/s)	−93.0 ± 17	−89.2 ± 15.8	0.14
Firing frequency at 200 pA (Hz)	33.0 ± 18.4	34.4 ± 20.5	0.77
Firing frequency at 500 pA (Hz)	72.6 ± 29.8	77.8 ± 42.1	0.68

Young mice (P14–20) and the K-gluconate-based internal solution were used for the experiments. Current-clamp recordings were performed at near physiological temperature (34 ± 1 °C).
Data are provided as the means ± standard deviation, and n = number of experiments.

2201 > WIN > JWH-018. These findings are consistent with our unpublished data on the IC50s for these synthetic cannabinoids, measured by a binding assay for human recombinant CB1Rs (see Discussion). IC50 of Δ^9-THC was not able to be calculated due to ambiguous fitting. These results demonstrate that MAM-2201 is a more potent inhibitor of PF-PC synaptic transmission than JWH-018 and Δ^9-THC.

3.4. MAM-2201 inhibits GABAergic synaptic transmission at inhibitory interneuron-PC synapses via presynaptic mechanisms

PCs receive feed-forward inhibition from GABAergic inhibitory interneurons lying in the molecular layer of the cerebellar cortex (Llinas et al., 2004), and this inhibition shapes the spike output of PCs (Mittmann et al., 2005). To explore how MAM-2201 modulates this inhibitory synaptic input, we recorded GABAergic synaptic transmission at inhibitory interneuron-PC synapses and examined the effects of MAM-2201 on inhibitory transmission. As shown in Fig. 5*B*, 10 μM MAM-2201 decreased the first IPSC amplitude (MAM-2201 in Fig. 5*Ba* and *Bb*; Fig. 5*C*, $n = 6$, $p < 0.001$), and a similar reduction was observed by 1 μM MAM-2201, indicating the MAM-2201-induced decrease was concentration-dependent (Fig. 5*C*, MAM-2201). MAM-2201 (10 μM) significantly increased PPR and CV (Scaled in Fig. 5*Ba*, *D* and *E*, MAM-2201), and these increases were comparable to those obtained by WIN (10 μM, Fig. 5*D* and *E*, WIN). Moreover, MAM-2201 (10 μM) decreased mIPSC frequency (IEI, Control: 451.2 ± 464.1 ms, MAM-2201: 718.8 ± 542.9 ms, $p < 0.05$, $n = 5$, Fig. 5*Fa* and *Fb*) without affecting mIPSC amplitude (peak amplitude, Control: 45.3 ± 22.3 pA, MAM-2201: 48.3 ± 24.1 pA, $p = 0.53$, $n = 5$, Fig. 5*Fa* and *Fc*). These results demonstrate that MAM-2201 inhibits GABAergic synaptic transmission at interneuron-PC synapses via presynaptic mechanisms.

3.5. MAM-2201-mediated presynaptic inhibition at CF-PC synapses reduces the number of spikelets in complex spikes and dendritic Ca^{2+} transients in PCs

Activation of CFs produces AMPA receptor-mediated strong postsynaptic depolarization and evokes an all-or-none spike with multiple peaks (spikelets), called "complex spikes" in the soma (Llinas et al., 2004). Complex spikes are accompanied by a large, dendritic Ca^{2+} transient, which plays a crucial role in producing long-term depression (LTD) at PF-PC synapses (Konnerth et al., 1992). At CF terminals, activation of presynaptic CB1Rs by WIN reduces glutamate release (Maejima et al., 2001). To examine how presynaptic modulation by MAM-2201 at CF-PC synapses affects the waveforms of complex spikes and CF-induced dendritic Ca^{2+} transients, we first confirmed presynaptic inhibition by MAM-2201 at CF-PC synapses (Fig. 6), and then performed simultaneous recordings of complex spikes and intracellular Ca^{2+} transients (Fig. 7).

First, CF-PC EPSCs were recorded at the holding potential of −10 mV in the presence of picrotoxin (Fig. 6*B–E*). To improve the space clamp in dendrites, young mice (P14–20) were used for the following experiments. This was because CF innervation of PCs is almost matured at this age (Hashimoto and Kano, 2013), and their dendrites are compact compared with those of adult (~P57) mice (McKay and Turner, 2005). As shown in Fig. 6*B* and *C*, bath application of MAM-2201 (1 or 10 μM) reduced CF-PC EPSC amplitude in a concentration-dependent manner. This reduction was accompanied by significant increases in PPR and CV (10 μM MAM-2201; Scaled in Fig. 6*Ba*, *C* and *D*). Moreover, MAM-2201 (10 μM) decreased CF-PC qEPSC frequency (IEI, Control: 176.5 ± 40.3 ms, MAM-2201: 234.5 ± 51.1 ms, $p < 0.01$, $n = 5$, Fig. 6*Fa* and *Fb*) without affecting CF-PC qEPSC amplitude (peak amplitude, Control: 22.5 ± 2.7 pA, MAM-2201: 22.0 ± 4.0 pA, $p = 0.75$, $n = 5$, Fig. 6*Fa* and *Fc*). These results indicate that MAM-2201 presynaptically inhibits neurotransmitter release from CF terminals.

We then simultaneously recorded complex spikes in the somata and Ca^{2+} transients in the dendrites of PCs using the K-gluconate-based internal solution containing OGB-1 at near physiological temperature. Complex spikes were elicited under current-clamp conditions. As presented in Fig. 7*A*, electrical stimulation of CFs evoked all-or-none complex spikes consisting of spikelets (Control in Fig. 7*A*). MAM-2201 (10 μM, 10 min) significantly reduced the number of spikelets to 78% of the control (Fig. 7*B*, $n = 11$, $p < 0.001$). Because MAM-2201 modulated synaptic properties via activation of presynaptic CB1Rs (Fig. 3), and because PCs do not express CB1Rs (Kano et al., 2009), we would not expect MAM-2201 to affect the intrinsic membrane properties of PCs. As expected, we were able to confirm that MAM-2201 did not affect the resting membrane potential, input resistance, or action potential properties of PCs (Table 2). Accordingly, MAM-2201-induced changes in complex spike waveforms can be interpreted based on depression of CF-PC EPSCs. The complex spikes evoked by CF stimulation were accompanied by large Ca^{2+} transients in the dendrites (Fig. 7*Cb*, Control). MAM-2201 substantially decreased the peak amplitude of the Ca^{2+} transient (Fig. 7*Cb*, MAM-2201). Both the peak and the integral of the Ca^{2+} transients were significantly attenuated by 10 μM MAM-2201 (peak: $n = 10$, $p < 0.01$, Fig. 7*Da*; integration: $n = 10$, $p < 0.01$, Fig. 7*Db*). Taken together, these results indicate that MAM-2201 alters PC responses to CF activation by reducing the number of spikelets and the dendritic Ca^{2+} transients. This implies that MAM-2201 would decrease complex spike-mediated information propagation from PCs to the next nuclei and might affect induction of intracellular Ca^{2+}-dependent LTD at PF-PC synapses (see Discussion).

4. Discussion

This is the first study of the effects of MAM-2201 on neuronal functions. We found that MAM-2201 acted as an agonist of CB1Rs (Fig. 2). We also found that MAM-2201 inhibited glutamatergic synaptic transmission presynaptically via activation of presynaptic CB1Rs (Fig. 3). At the same concentrations, MAM-2201 decreased PF-PC EPSCs more potently than JWH-018 and Δ^9-THC (Fig. 4). Moreover, MAM-2201 also presynaptically suppressed GABAergic synaptic transmission at interneuron-PC synapses (Fig. 5) and glutamatergic synaptic transmission at CF-PC synapses (Fig. 6). In the case of smaller CF-PC EPSCs, MAM-2201 led to reduction of the number of action potentials in complex spikes and to reduced